bioRxiv preprint doi: https://doi.org/10.1101/2021.12.13.472341; this version posted September 28, 2022. The copyright holder for this preprint (which was not certified by peer review) is the author/funder, who has granted bioRxiv a license to display the preprint in perpetuity. It is made available under aCC-BY 4.0 International license.

Title

Automated image analysis method to detect and quantify fat cell infiltration in hematoxylin and eosin stained human pancreas histology images

Authors

Roshan Ratnakar Naik[1], Annie Rajan[2], Nehal Kalita[3]

Affiliations

[1] Dr. Roshan Ratnakar Naik, Assistant Professor, Department of Biotechnology, Parvatibai Chowgule College of Arts & Science, Margao-Goa, 403601. ORCID ID: 0000-0003-4515-871X. Email address: ros007swa@gmail.com

[2] Mrs. Annie Rajan, Associate Professor, Department of Computer Science and Technology, Dhempe College of Arts and Science, Miramar, Panaji-Goa, 403 001. ORCID ID: 0000-0001-6201-2654. Email address: ann_raj_2000@yahoo.com

[3] Nehal Kalita, M.Sc. Computer Science. ORCID ID: 0000-0001-6997-5621. Email address: nehalkalita94@gmail.com

Corresponding Author: Dr. Roshan R. Naik

Author contributions

R.R.N. conceptualized the idea and wrote the manuscript.

A.R. conceptualized the idea.

N.K. formulated the mathematical approach and wrote the Python programs.

bioRxiv preprint doi: https://doi.org/10.1101/2021.12.13.472341; this version posted September 28, 2022. The copyright holder for this preprint (which was not certified by peer review) is the author/funder, who has granted bioRxiv a license to display the preprint in perpetuity. It is made available under aCC-BY 4.0 International license.

Abstract

Fatty infiltration in pancreas leading to steatosis is a major risk factor in pancreas transplantation. Hematoxylin and eosin (H and E) is one of the common histological staining techniques that provides information on the tissue cytoarchitecture. Adipose (fat) cells accumulation in pancreas has been shown to impact beta cell survival, its endocrine function and pancreatic steatosis and can cause non-alcoholic fatty pancreas disease (NAFPD). The current automated tools (E.g. Adiposoft) available for fat analysis are suited for white adipose tissue which is homogeneous and easier to segment unlike heterogeneous tissues such as pancreas where fat cells continue to play critical physiopathological functions. The currently, available pancreas segmentation tool focuses on endocrine islet segmentation based on cell nuclei detection for diagnosis of pancretic cancer. In the current study, we present a fat quantifying tool, Fatquant, which identifies fat cells in heterogeneous H and E tissue sections with reference to diameter of fat cell. Using histological images of pancreas from a publicly available database, we observed an intersection over union of 0.797 to 0.966 for manual versus fatquant based machine analysis.

Keywords

Adipose or fat cells, Hematoxylin and Eosin, image processing, tissue segmentation, pancreas, liver

Author Summary

We have developed an automated tool, Fatquant, for identification of fat cells based on its diameter in complex hematoxylin and eosin tissue sections such as pancreas which can aid the pathologist for diagnosis of fatty pancreas and related metabolic conditions. Fatquant is unique as current fat automated tools (adiposoft, adipocount) works well for homogeneous white

bioRxiv preprint doi: https://doi.org/10.1101/2021.12.13.472341; this version posted September 28, 2022. The copyright holder for this preprint (which was not certified by peer review) is the author/funder, who has granted bioRxiv a license to display the preprint in perpetuity. It is made available under aCC-BY 4.0 International license.

adipose tissue but not for other tissue samples. The currently available pancreas analysis tool are mostly suited for segmentation of endocrine β-cell based on cell nuclei detection, extracting colour features and cannot estimate fat cell infiltration in pancreas.

Graphical Abstract

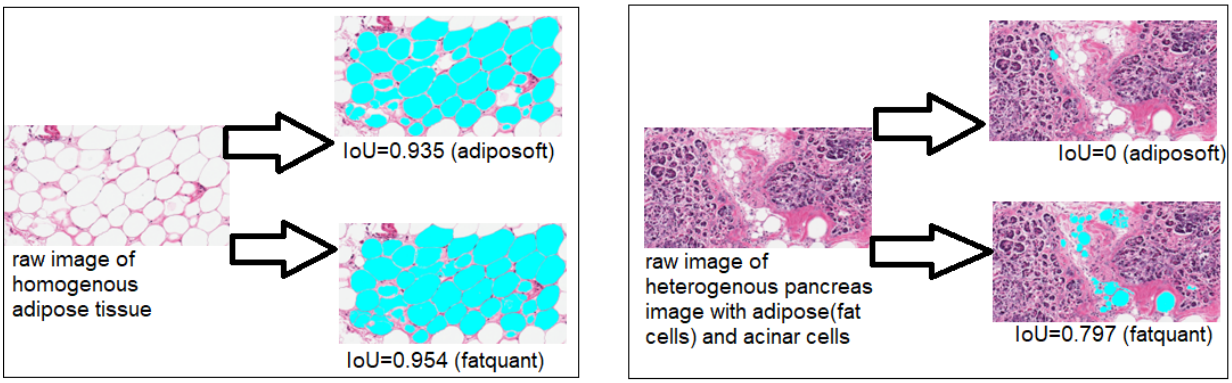

Currently available fat quantification tools like adiposoft can analyze homogenous adipose tissue (left) with intersection over union (IoU) of 0.935 and 0.954 with adiposoft and fatquant, respectively. While in heterogenous tissue (e.g. pancreas on right) which contains adipose (fat cells), acinar cells, adiposoft fails to detect fat cells with IoU=0 while fatquant had IoU=0.797.

1. Introduction

The accumulation of fats especially in the abdominal area causes insulin resistance leading to deposition of fats (steatosis) in the pancreas, inflammation and finally fibrosis leading to non-alcoholic fatty pancreatic disease (NAFPD). Accumulation of pancreatic fat may lead to pancreatitis, diabetes mellitus or pancreatic cancer (Paul and Shihaz 2020). Pancreatic steatosis can be diagnosed on ultrasound, computed tomography (CT) scan or magnetic resonance imaging (MRI) but pancreatic biopsy remains best method to detect pancreatic fat concentration (Tariq et al 2016, Paul and Shihaz 2020). The consequence of pancreatic fat infiltration might provoke a decrease in endocrine (β-cell) number and function, leading to more rapid progression to diabetes (Yu and Wang 2017). Sudies suggest NAFPD as an early marker of glucometabolic disturbance (Yu and Wang 2017). Pancreas transplantation is the only way to treat type 1

bioRxiv preprint doi: https://doi.org/10.1101/2021.12.13.472341; this version posted September 28, 2022. The copyright holder for this preprint (which was not certified by peer review) is the author/funder, who has granted bioRxiv a license to display the preprint in perpetuity. It is made available under aCC-BY 4.0 International license.

diabetes (T1D) but fat infiltration in pancreas remains a risk factor that can affect the clinical outcome (Verma and Papalois 2011, Dholakia et al 2017). Fatty pancreas has a prevalence of 35% and may be contributing factor for the malignancy and the metabolic syndrome (Lesmana et al 2015). The histological and MRI tools exhibit good agreement in detecting fat in pancreas (Fukui et al 2019, Virostko 2020) but the latter cannot show fat accumulation at the cellular level and is expensive. Decrease in fat content in liver and pancreas was associated with non-diabetic blood glucose control in people with type 2 diabetes (Taylor et al 2018).

Hematoxylin and eosin (H & E) is a widely used histological tissue staining technique for medical diagnosis and scientific research. Hematoxylin stains cell nuclei blue while eosin stains the cytoplasm and connective tissue pink thus allowing microscopic differentiation of tissue cytoarchitecture in sections. The analysis involves manual examination by pathologist to ascertain presence/absence of disease markers and or grading of disease progression which is semi-quantitative and subjective in nature (Gurcan et al 2009).

To complement the current manual assessment, several digital tools have been developed such as Adiposoft (Galarraga et al 2012), and AdipoCount (Zhi et al 2018). However, they cannot efficiently identify fat cells in complex tissues such as pancreas or liver as white adipose tissue is generally homogeneous (Figure 1) making tissue segmentation relatively easier (Glastonbury et al 2020). Such tool developed based on nuclear displacement and lipid droplet size analysis exists for automated analysis of fat cell infiltration (steatosis) in H and E liver images (Nativ et al 2014). Unlike liver tissue, where fats accumulate in hepatocytes, in pancreas fat infiltration and deposition occurs both in acinar and islet cells (Catanzaro et al 2016). The ratio of accumulated pancreatic fat area relative to exocrine gland (acinar and duct tissue) area was significantly increased in obese mice model (Matsuda et al 2014).

Usually, these algorithms involve splitting the image into various color channels with the red channel binarized using automatic thresholding method to separate the bright pink fat areas from

bioRxiv preprint doi: https://doi.org/10.1101/2021.12.13.472341; this version posted September 28, 2022. The copyright holder for this preprint (which was not certified by peer review) is the author/funder, who has granted bioRxiv a license to display the preprint in perpetuity. It is made available under aCC-BY 4.0 International license.

dark purple-bluish cell nuclei. Subsequently, a watershed algorithm is applied to fillup missing fat cell membrane and improves cell count (Galarraga et al 2012, Zhi et al 2018). The output of these processes includes the labels and statistical analysis of individual cells. These tools have been successfully applied to white adipose tissue, however, other organs like liver, pancreas, lungs have been challenging due to heterogeneous cell types (Figure 2).

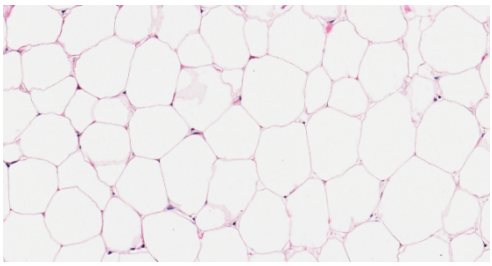

Figure 1-Homogenous adipose tissue

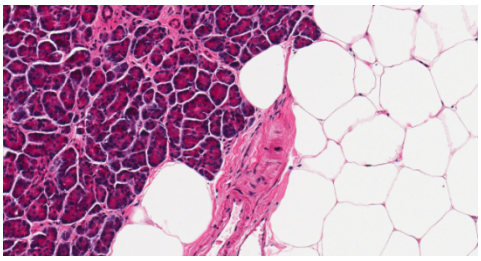

Figure 2-Heterogenous pancreatic tissue with adipose and acinar cells

Pancreas is a heterogenous tissue and manual analysis of regions is a tedious process that lacks reproducibility (Apaolaza et al 2021). The existing methods of pancreatic islet segmentation depends on cell nuclei detection, then a classifier is applied to recognize different cell types but is based on assumption that islets have high density cells (Floros et al 2009, Rechsteiner et al 2014). Recent studies have utilized a supervised learning framework for islet segmentation in H & E stained pancreatic images to partition images into superpixels and extract color-texture features, process them, and finally a linear support vector machine is trained and applied to segment testing images (Huang et al 2016). Moreover, QuPath software allows identification of endocrine islet cells in immunofluorescent images of pancreas tissue (Apaolaza et al 2021), but these tools does not allow quantification of adipose (fat) cells in pancreatic images. In the current study, we have developed an automated tool, Fatquant, in which the fat cells were identified in processed images by calculating the diagonal of a square circumscribed by circle.

bioRxiv preprint doi: https://doi.org/10.1101/2021.12.13.472341; this version posted September 28, 2022. The copyright holder for this preprint (which was not certified by peer review) is the author/funder, who has granted bioRxiv a license to display the preprint in perpetuity. It is made available under aCC-BY 4.0 International license.

2. Materials and Methods

The H and E images for the analysis were downloaded from a publicly accessible Genotype-Tissue Expression (GTEx) Portal (Broad Institute, Cambridge, MA, USA) using the Histology Viewer tool (Consortium 2015). The GTEx tissue image library contains high-resolution histology images for various tissue types from several postmortem donors. Spherical or oval white spaces were categorized as fat (adipose) cells while large and irregular white spaces were grouped as artifacts. A sample size of ten pancreas histology images were analyzed from slide IDs GTEX-11DXZ-0826, GTEX-1122O-0726, GTEX-1117F-1726, GTEX-117YW-0926, GTEX-13PVQ-2026, GTEX-13FHP-1926 and GTEX-11WQC-0926. The images have magnification of 20x (0.4942 mpp—microns per pixel) (Badea and Stanescu 2020). The sample images were taken using the Snapshot tool of Aperio ImageScope software. The source code was written in Python version 3.8.0 (Python Software Foundation, Beaverton, Oregon, USA) with Core i7 3rd Generation CPU, 8 GB RAM and Intel HD graphics 4000 GPU.

2.1. Data and code availability

All the images, annotations along with relevant data code can be found at the following GitHub repository: https://github.com/anniedhempe/Fatquant. The procedure to run this tool is mentioned in the Readme file.

2.2. Image processing

bioRxiv preprint doi: https://doi.org/10.1101/2021.12.13.472341; this version posted September 28, 2022. The copyright holder for this preprint (which was not certified by peer review) is the author/funder, who has granted bioRxiv a license to display the preprint in perpetuity. It is made available under aCC-BY 4.0 International license.

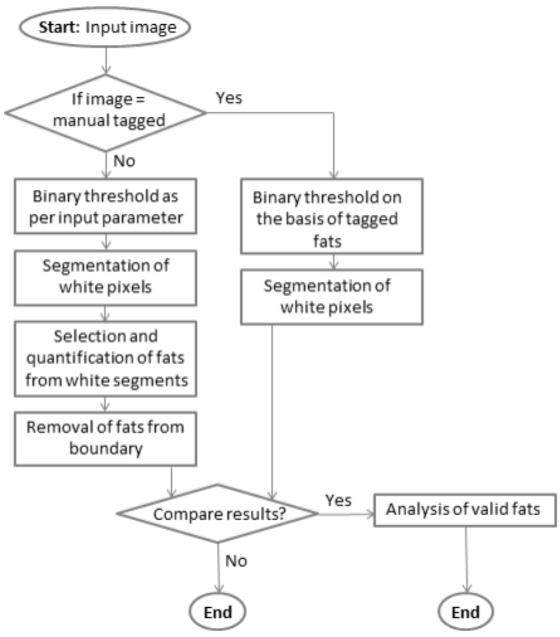

Figure 3: Flowchart depicting the image processing.

The procedure for image processing is briefly demonstrated in the flow chart shown in Figure 3.

The steps used are elaborated below.

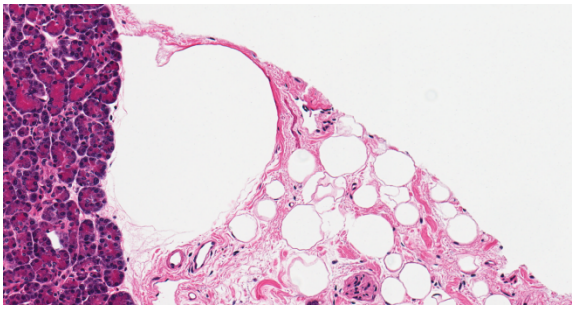

Figure 4

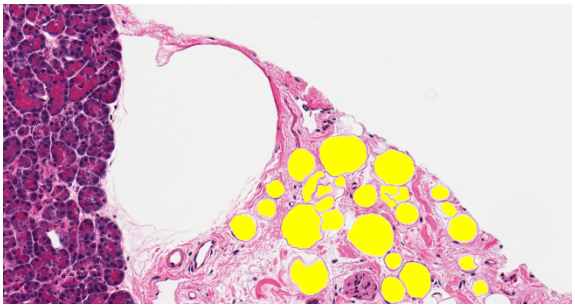

Figure 5

Figure 4 is a sample raw image of dimension 1716 x 905 pixels from whole slide GTEX-11DXZ-0826. Analysis on this image is referred while explaining the image processing steps. Figure 5 is an altered form of the image in Figure 4 where the valid fat cells are manually tagged with yellow color (RGB: 255, 255, 0).

bioRxiv preprint doi: https://doi.org/10.1101/2021.12.13.472341; this version posted September 28, 2022. The copyright holder for this preprint (which was not certified by peer review) is the author/funder, who has granted bioRxiv a license to display the preprint in perpetuity. It is made available under aCC-BY 4.0 International license.

2.2.1. Binary thresholding of input image

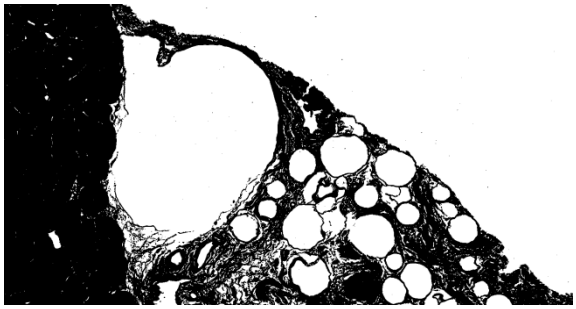

Figure 6

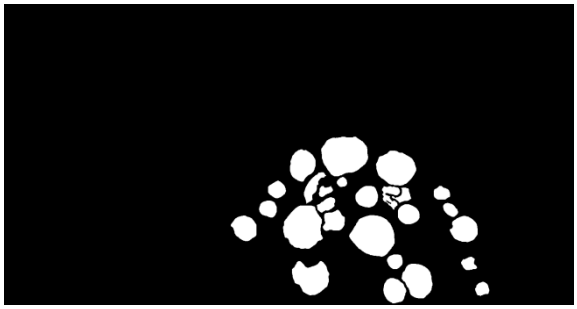

Figure 7

The color of fat cells in images from GTEX portal ranges approximately between 225 to 255 grayscale values. There can also be other parts of pancreas which has the same range of color. But applying binary threshold on an image can help in getting rid of many unwanted parts. The pixels of an image whose color values are at least equal to the input parameter value of threshold (e.g. 227) are taken into consideration for further processing and are assigned a new grayscale value 255. The other pixels are assigned value 0. Figure 6 is a thresholded image of Figure 4 with parameter value 230. Figure 7 is also a thresholded image but of Figure 5 where pixels representing the tagged fat cells are assigned grayscale value 255 and the rest is assigned value 0.

2.2.2. Segmentation of white pixels from thresholded image

White pixels are initially segmented by combining tile rendering with scanline rendering and then identifying possible merge of segments in a tile with their immediate neighbors. Tile rendering has been implemented in this system as it helps in reducing time complexity for segments covering large area.

Processing time for segmentation was tested with four sizes of square tiles, which were of length 35 pixels (processing time: 24.23 seconds), 50 pixels (processing time: 15.32 seconds), 70 pixels (processing time: 12.88 seconds) and 100 pixels (processing time: 15.37 seconds). In this experiment, tile size of 70 pixels was used for analyzing all the images since it took the least

bioRxiv preprint doi: https://doi.org/10.1101/2021.12.13.472341; this version posted September 28, 2022. The copyright holder for this preprint (which was not certified by peer review) is the author/funder, who has granted bioRxiv a license to display the preprint in perpetuity. It is made available under aCC-BY 4.0 International license.

amount of time.

After an input image is divided into multiple tiles, scanline rendering is performed within each tile to identify white pixels and form possible segments with their neighbors on left or top. In this experiment, left neighbors are given first preference. Once scanline rendering is performed till the last row of a tile then the identified segments are merged on the basis of their vertical neighbors. Segments which have only diagonal neighbors with another segment and not vertical, are not merged.

Figure 8 is a diagrammatic representation of segmentation performed on a square tile of length 15 pixels. Figure 8 (a) represents a thresholded image where segmentation is to be performed. Figure 8 (b) shows six segments created while iterating once till the last row. Figure 8 (c) shows total segments getting reduced to four due to merging.

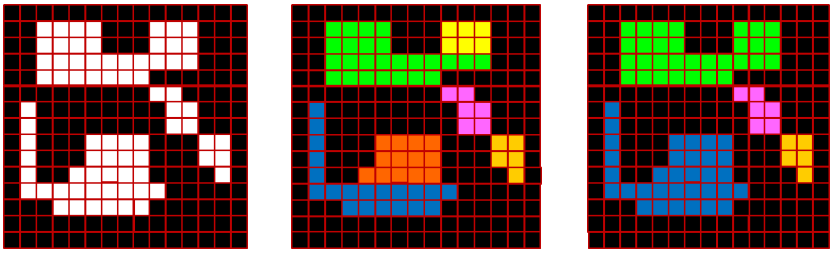

Figure 8 (a) **Figure 8 (b)** **Figure 8 (c)**

Figure 9 shows segments within tiles and the magnified part is one tile. Figure 10 shows fully merged segments of the thresholded image and varying colors (non-black) in it represent different segments.

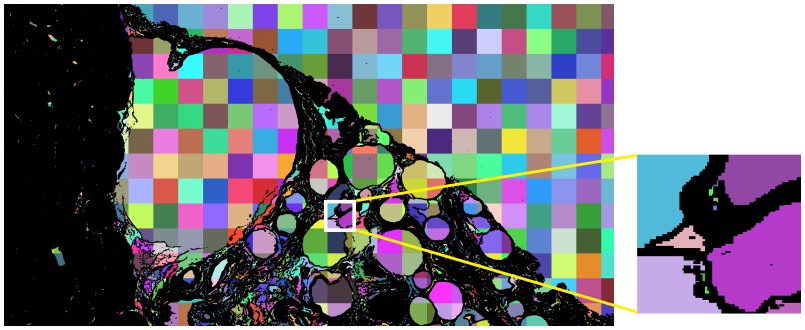

Figure 9

bioRxiv preprint doi: https://doi.org/10.1101/2021.12.13.472341; this version posted September 28, 2022. The copyright holder for this preprint (which was not certified by peer review) is the author/funder, who has granted bioRxiv a license to display the preprint in perpetuity. It is made available under aCC-BY 4.0 International license.

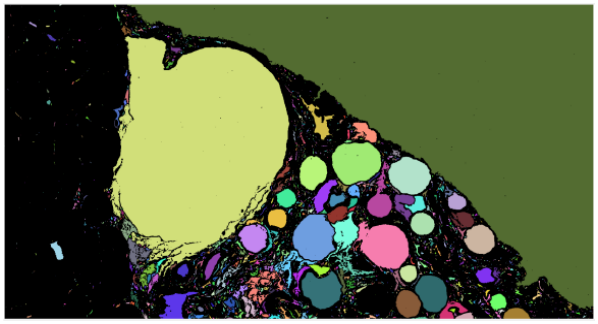

Figure 10

2.2.3. Selection and quantification of fats from white segments

The system uses image kernel to select probable valid segments. But before applying kernel, the system determines the smallest dimension that encompasses all the segments. The kernel's position is only updated by one pixel (horizontally or vertically) in each iteration so determining the smallest dimension for traversal reduces the time complexity. This dimension is determined by identifying positions of first white pixels in thresholded image from every direction (i.e. top, bottom left and right). These four positions denote maximum coverage of segments in each direction. Figure 11 is a diagrammatic representation of the method discussed where the Red colored rectangle represents smallest dimension.

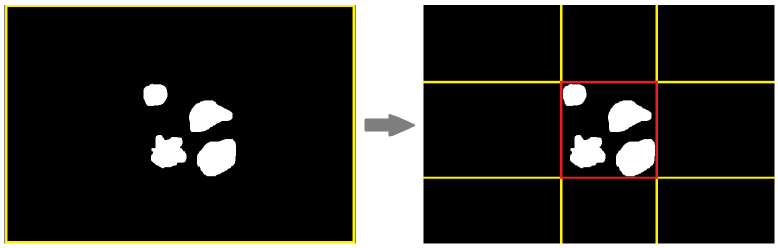

Figure 11

The system uses a square shaped kernel which is supposed to fit inside the boundaries of valid segments. The side length of that square is determined by input fat diameter values (minimum or maximum) as these diameters equates to diagonal of that square. Side length of a square, can be calculated as:

s =d divided by square root of 2.

bioRxiv preprint doi: https://doi.org/10.1101/2021.12.13.472341; this version posted September 28, 2022. The copyright holder for this preprint (which was not certified by peer review) is the author/funder, who has granted bioRxiv a license to display the preprint in perpetuity. It is made available under aCC-BY 4.0 International license.

$$s = \frac{d}{\sqrt{2}}$$

, where s = square side length; d = diameter. This square can be assumed as the largest square that can get inscribed in a circle of given diameter. An elliptical kernel may be a more precise choice for identifying fats but since square kernel is easier to handle so it has been chosen.

The system refers to a minimum diameter value to select segments where a square kernel having side length as per this diameter can fit somewhere in their regions. Then the system refers to a maximum diameter value to discard segments from the selected list where a kernel having side length as per this diameter can fit somewhere in their regions. This means a segment which has narrow areas in many of its portions, but has very wide area in one of its portion can also get discarded if a square kernel as per the maximum diameter can fit in that portion. Figure 12 is a diagrammatic representation of this process performed on an image of dimension 15 x 15 pixels. Figure 12 (a) has seven segments with White colored pixels out of which valid segments are to be selected. Figure 12 (b) has three segments marked with Cyan color which denotes segments getting selected as per minimum diameter. The kernel size is of length 3 pixels. So, four segments do not get selected as the square kernel fails to fit inside the boundary of any of these segments. Figure 12 (c) has only two segments marked with Cyan color which denotes selected segment getting discarded as per maximum diameter. Here the kernel size is of length 4 pixels. So, a segment which can fit a kernel of length greater than 4 pixels is to be discarded. The previously selected segment which gets discarded could fit a kernel of length 5 pixels. Figures 13 (a) and (b) are outputs generated from the sample image with minimum (27 pixels) and maximum (130 pixels) diameter respectively. The identified fats are marked with Cyan color (RGB: 0, 255, 255).

bioRxiv preprint doi: https://doi.org/10.1101/2021.12.13.472341; this version posted September 28, 2022. The copyright holder for this preprint (which was not certified by peer review) is the author/funder, who has granted bioRxiv a license to display the preprint in perpetuity. It is made available under aCC-BY 4.0 International license.

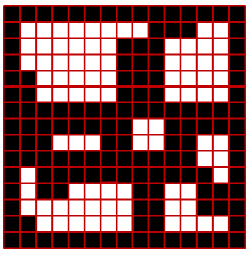

Figure 12 (a)

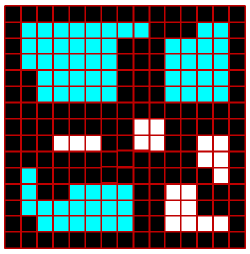

Figure 12 (b)

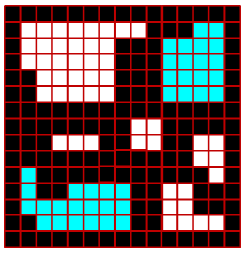

Figure 12 (c)

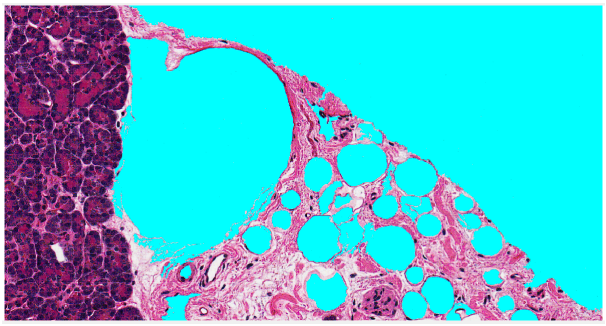

Figure 13 (a)

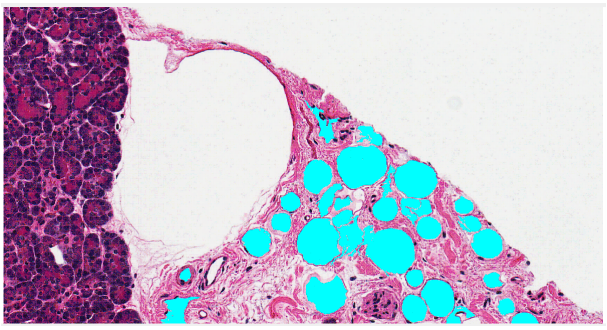

Figure 13 (b)

2.2.4. Removal of fats from boundary

Segments which are identified as fats but also contain pixels from boundary are discarded because their entire size is not known within the dimension of input image (Figure 14). While comparing Figure 14 with Figure 13 (b), it can be seen that some segments which contain pixels from bottom boundary gets discarded.

Some of these segments may even get discarded while selecting segments as per diameter. E.g. in Figure 13 (b), one big segment which has pixels in boundary gets discarded after considering maximum diameter area, whereas the segment is present in Figure 13 (a).

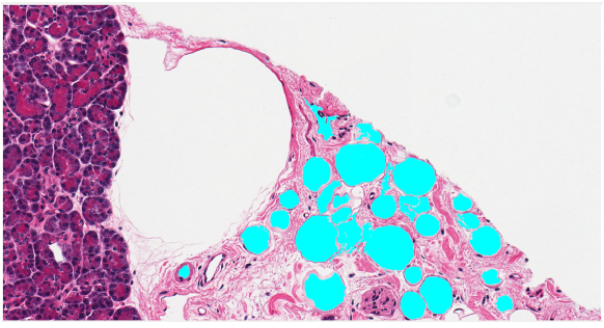

Figure 14: Fat cell removed from peripheral boundary.

bioRxiv preprint doi: https://doi.org/10.1101/2021.12.13.472341; this version posted September 28, 2022. The copyright holder for this preprint (which was not certified by peer review) is the author/funder, who has granted bioRxiv a license to display the preprint in perpetuity. It is made available under aCC-BY 4.0 International license.

Removing fats from boundaries is the final step for tagging fats using machine. If users do not have manual tagged data of fat cells then they can conclude the experiment after this step.

2.2.5. Analysis of valid fats

The machine tagged fat segments are compared with manually tagged fat segments to check the validity of our image analysis algorithm. If machine and manually tagged segments have pixels in common then, those pixels are considered as valid. The accuracy of the output is calculated in terms of Intersection over Union (IoU). The formula is:

$$IoU = \frac{TP}{FP + TP + FN}$$

, where TP = True Positive; FP = False Positive; FN = False Negative. TP is the intersection of machine and manually tagged pixels, FP are the pixels which are tagged by machine but do not become part of the intersection (i.e. Machine Tagged Area - TP) and FN are the pixels which are manually tagged but do not become part of the intersection (i.e. Manual Tagged Area - TP).

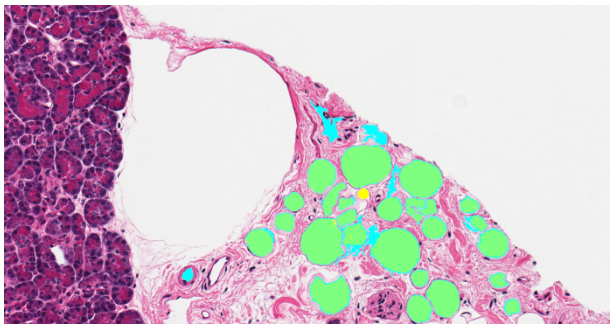

Figure 15

Figure 15 is the output generated after comparing machine and manual tagged fats. The Light Green colored pixels (RGB: 127, 255, 127) represents TP, Cyan color represents FN and Yellow color represents FP. Machine tagged, manual tagged and TP areas are 130,816, 111,300 and 110,429 pixels respectively. Hence as per the parameters used while demonstrating the steps, the IoU value is 0.838 but it can increase if parameters are changed or a better manual tagged image is referred.

3. Results

bioRxiv preprint doi: https://doi.org/10.1101/2021.12.13.472341; this version posted September 28, 2022. The copyright holder for this preprint (which was not certified by peer review) is the author/funder, who has granted bioRxiv a license to display the preprint in perpetuity. It is made available under aCC-BY 4.0 International license.

Fat cell identification on ten sample images of dimension 1716 x 905 pixels was performed using Adiposoft and Fatquant tools. The outputs are shown below.

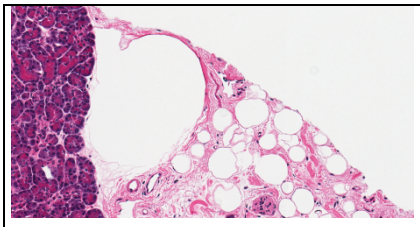

Figure 16 (a)-Raw image

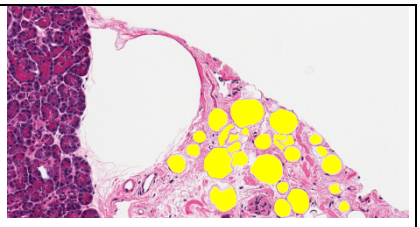

Figure 16 (b)-Tagged image

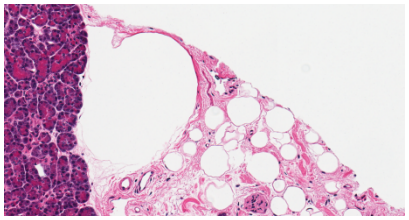

Figure 16 (c)-Adiposoft

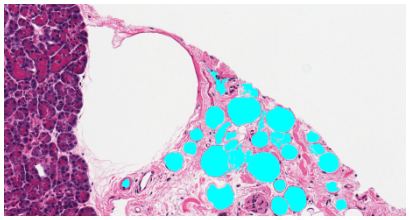

Figure 16 (d)-Fatquant

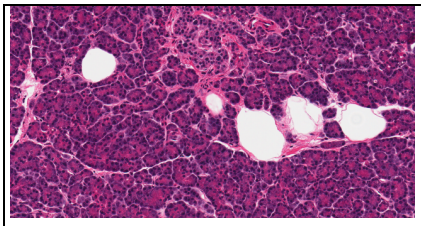

Figure 17 (a)- Raw image

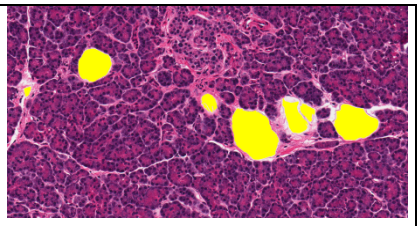

Figure 17 (b)- Tagged image

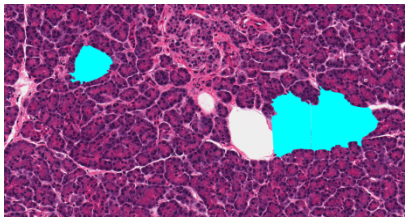

Figure 17 (c)- Adiposoft

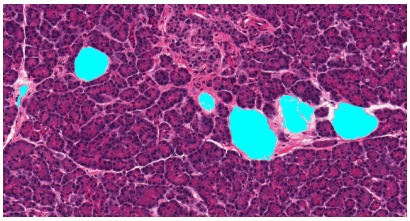

Figure 17 (d)-Fatquant

bioRxiv preprint doi: https://doi.org/10.1101/2021.12.13.472341; this version posted September 28, 2022. The copyright holder for this preprint (which was not certified by peer review) is the author/funder, who has granted bioRxiv a license to display the preprint in perpetuity. It is made available under aCC-BY 4.0 International license.

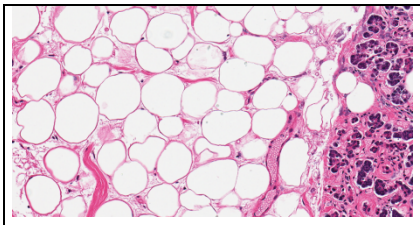

Figure 18 (a)- Raw image

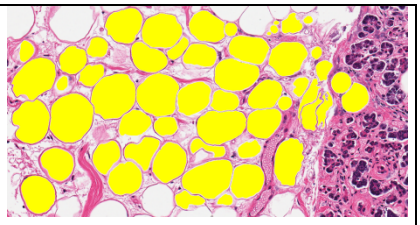

Figure 18 (b)- Tagged image

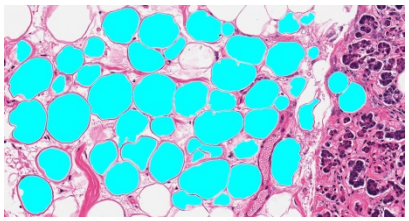

Figure 18 (c)- Adiposoft

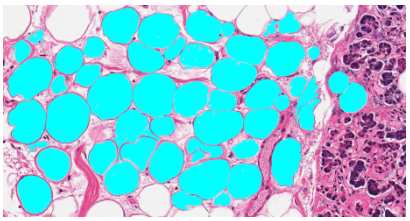

Figure 18 (d)-Fatquant

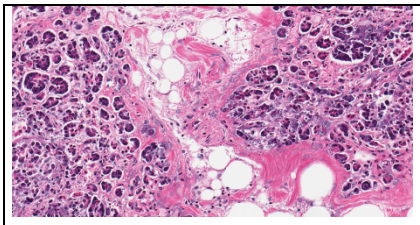

Figure 19 (a)- Raw image

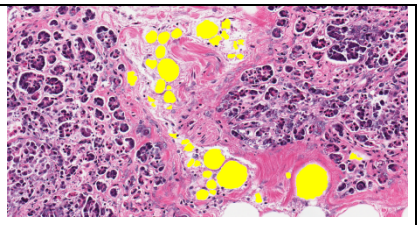

Figure 19 (b)- Tagged image

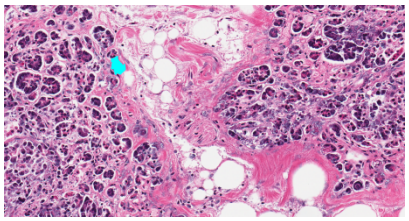

Figure 19 (c)- Adiposoft

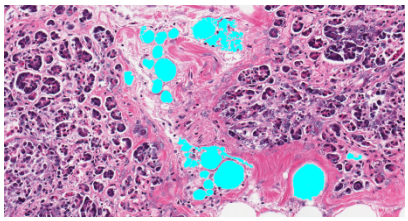

Figure 19 (d)-Fatquant

bioRxiv preprint doi: https://doi.org/10.1101/2021.12.13.472341; this version posted September 28, 2022. The copyright holder for this preprint (which was not certified by peer review) is the author/funder, who has granted bioRxiv a license to display the preprint in perpetuity. It is made available under aCC-BY 4.0 International license.

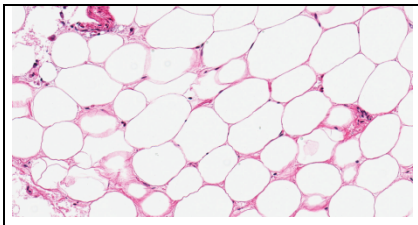

Figure 20 (a)- Raw image

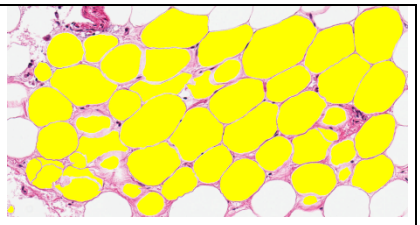

Figure 20 (b)- Tagged image

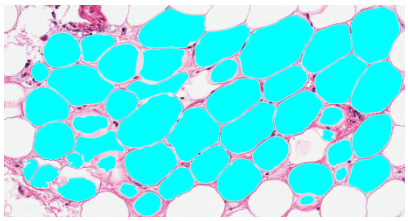

Figure 20 (c)- Adiposoft

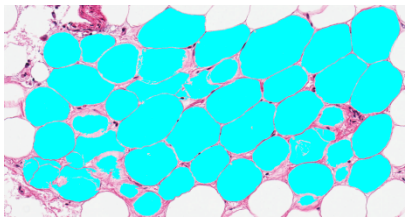

Figure 20 (d)-Fatquant

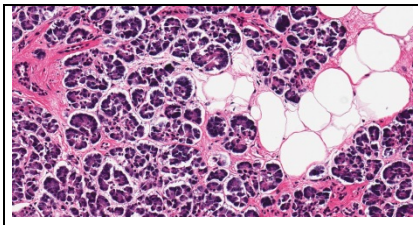

Figure 21 (a)- Raw image

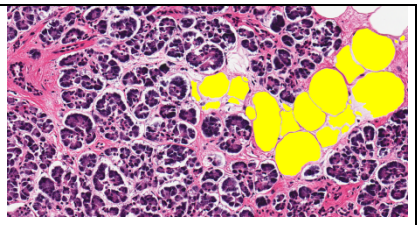

Figure 21 (b)- Tagged image

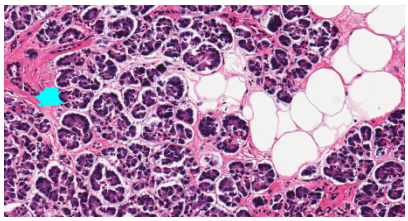

Figure 21 (c)- Adiposoft

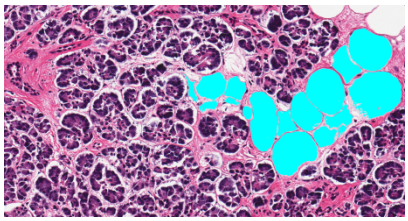

Figure 21 (d)-Fatquant

bioRxiv preprint doi: https://doi.org/10.1101/2021.12.13.472341; this version posted September 28, 2022. The copyright holder for this preprint (which was not certified by peer review) is the author/funder, who has granted bioRxiv a license to display the preprint in perpetuity. It is made available under aCC-BY 4.0 International license.

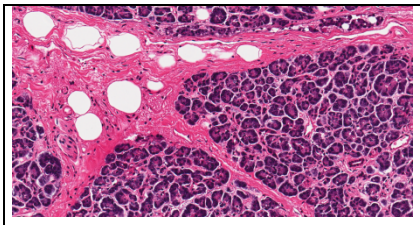

Figure 22 (a)- Raw image

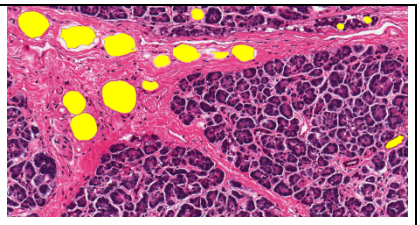

Figure 22 (b)- Tagged image

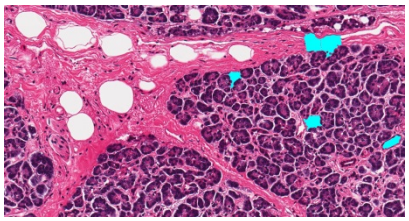

Figure 22 (c)- Adiposoft

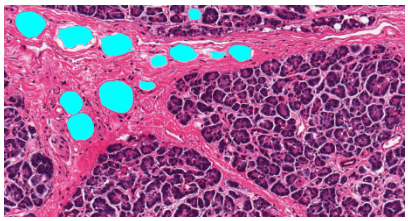

Figure 22 (d)-Fatquant

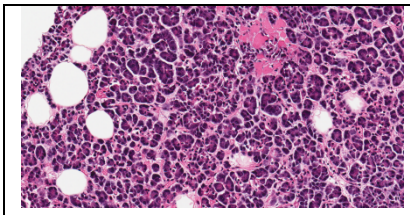

Figure 23 (a)- Raw image

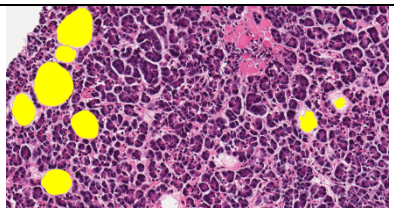

Figure 23 (b)- Tagged image

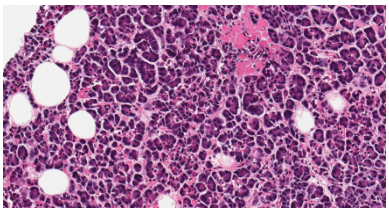

Figure 23 (c)- Adiposoft

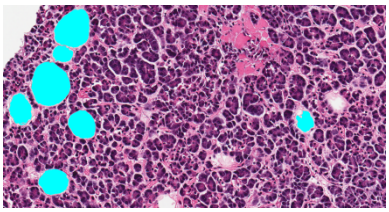

Figure 23 (d)-Fatquant

bioRxiv preprint doi: https://doi.org/10.1101/2021.12.13.472341; this version posted September 28, 2022. The copyright holder for this preprint (which was not certified by peer review) is the author/funder, who has granted bioRxiv a license to display the preprint in perpetuity. It is made available under aCC-BY 4.0 International license.

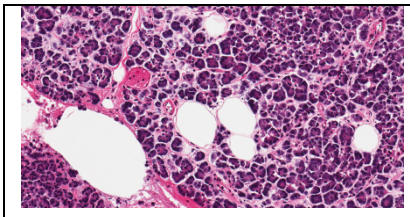

Figure 24 (a)- Raw image

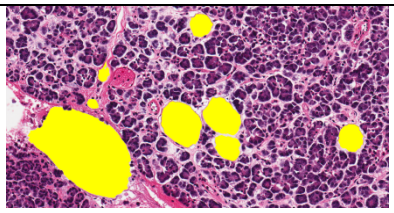

Figure 24 (b)- Tagged image

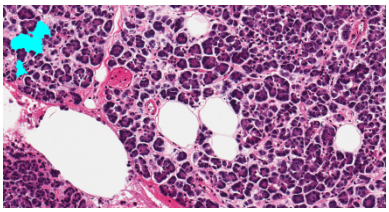

Figure 24 (c)- Adiposoft

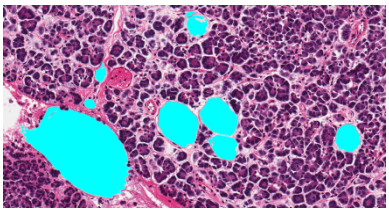

Figure 24 (d)-Fatquant

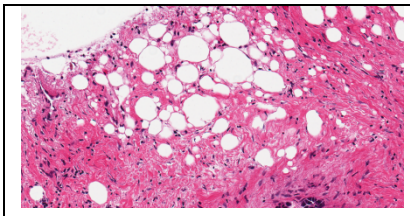

Figure 25 (a)- Raw image

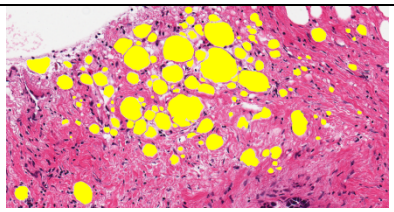

Figure 25 (b)- Tagged image

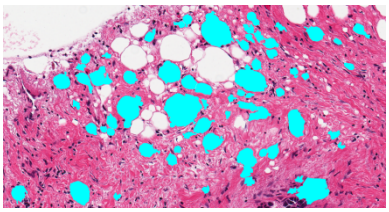

Figure 25 (c)- Adiposoft

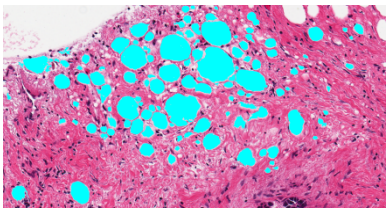

Figure 25 (d)-Fatquant

Table 1: Parameters used by tools in Figures 16 – 25

Figures	Samples	GTEx slide ID	Adiposoft			Fatquant		
			Microns per	Min. diameter	Max. diameter	Threshold value	Min. diameter	Max. diameter

bioRxiv preprint doi: https://doi.org/10.1101/2021.12.13.472341; this version posted September 28, 2022. The copyright holder for this preprint (which was not certified by peer review) is the author/funder, who has granted bioRxiv a license to display the preprint in perpetuity. It is made available under aCC-BY 4.0 International license.

			pixel					
16	1	11DXZ-0826	0.4942	20	135	230	27	130
17	2	1122O-0726	0.4942	25	500	228	25	500
18	3	1117F-1726	0.4942	22	500	228	29	500
19	4	1117F-1726	0.4942	20	180	233	24	150
20	5	117YW-0926	0.4942	20	280	231	24	250
21	6	117YW-0926	0.4942	22	280	229	27	250
22	7	13PVQ-2026	0.4942	22	250	226	29	200
23	8	13FHP-1926	0.4942	40	300	228	40	250
24	9	13FHP-1926	0.4942	22	550	228	22	500
25	10	11WQC-0926	0.4942	14	200	231	14	200

Table 2: Calculation of accuracy on pancreas sample images

Samples	Tool	TP (in pixels)	FP (in pixels)	FN (in pixels)	IoU

bioRxiv preprint doi: https://doi.org/10.1101/2021.12.13.472341; this version posted September 28, 2022. The copyright holder for this preprint (which was not certified by peer review) is the author/funder, who has granted bioRxiv a license to display the preprint in perpetuity. It is made available under aCC-BY 4.0 International license.

1	Fatquant	110429	20387	871	0.838
	Adiposoft	0	0	111300	0
2	Fatquant	81041	5597	468	0.930
	Adiposoft	46769	60732	34740	0.329
3	Fatquant	591209	49758	11326	0.906
	Adiposoft	571949	14599	30586	0.927
4	Fatquant	72793	13053	5455	0.797
	Adiposoft	0	3245	78248	0
5	Fatquant	899818	35098	8576	0.954
	Adiposoft	851499	2285	56895	0.935
6	Fatquant	195357	5405	3457	0.957
	Adiposoft	0	6674	198814	0
7	Fatquant	81834	146	5830	0.932
	Adiposoft	2065	14838	85599	0.020
8	Fatquant	91516	1106	2498	0.962
	Adiposoft	0	0	94014	0
9	Fatquant	192031	2780	4020	0.966
	Adiposoft	0	15468	196051	0
10	Fatquant	219816	13070	8254	0.912
	Adiposoft	134342	64357	93728	0.459

Table 3: Fatquant parameters for liver sample images

Samples	Threshold value	Min. diameter	Max. diameter
000	205	50	150

bioRxiv preprint doi: https://doi.org/10.1101/2021.12.13.472341; this version posted September 28, 2022. The copyright holder for this preprint (which was not certified by peer review) is the author/funder, who has granted bioRxiv a license to display the preprint in perpetuity. It is made available under aCC-BY 4.0 International license.

010	205	28	220
036	211	34	150
058	210	45	200
090	207	40	140
116	207	45	200
120	207	40	200
196	216	40	200
212	203	35	300
319	212	32	100
335	220	31	150
385	218	23	220
421	215	20	130
440	215	30	150
498	208	38	180
515	212	34	220
555	215	42	220
596	215	36	180
610	213	22	180
723	212	32	150

The threshold value, minimum and maximum diameter were chosen to get an optimal output.

Table 4: Calculation of accuracy using Fatquant on liver sample images

Samples	TP (in pixels)	FP (in pixels)	FN (in pixels)	IoU
000	27496	5223	97	0.838
010	66999	10834	2419	0.835

bioRxiv preprint doi: https://doi.org/10.1101/2021.12.13.472341; this version posted September 28, 2022. The copyright holder for this preprint (which was not certified by peer review) is the author/funder, who has granted bioRxiv a license to display the preprint in perpetuity. It is made available under aCC-BY 4.0 International license.

036	21561	3940	129	0.841
058	39343	5233	91	0.881
090	61281	8386	510	0.873
116	50354	9816	607	0.828
120	65042	10587	94	0.859
196	119188	9727	2547	0.907
212	62885	12752	298	0.828
319	20594	6103	511	0.757
335	45856	10862	1614	0.786
385	56330	9776	1268	0.836
421	73060	12052	326	0.855
440	28788	4726	677	0.842
498	63565	12067	1301	0.826
515	96819	12566	1514	0.873
555	69386	12856	1222	0.831
596	21020	4502	528	0.807
610	52206	10069	1852	0.814
723	12971	3286	436	0.777

Additionally, we analyzed liver images (Roy et al 2020) using our fatquant tool with IoU of 0.757 to 0.907 indicating wide applicability of our tool

Image (a) in Figures 16 – 25 are the raw sample images; (b) are manual fat tagged images; (c) and (d) are outputs from Adiposoft and Fatquant respectively. The parameter values of Adiposoft and Fatquant (mentioned in Table 1) are not exactly same because the default threshold or edge detection values used by Adiposoft are unknown to users. Hence for analysis, values have been

bioRxiv preprint doi: https://doi.org/10.1101/2021.12.13.472341; this version posted September 28, 2022. The copyright holder for this preprint (which was not certified by peer review) is the author/funder, who has granted bioRxiv a license to display the preprint in perpetuity. It is made available under aCC-BY 4.0 International license.

chosen as per optimal output. Pixels being part of fat in (b) are marked with yellow color whereas pixels identified as fat in (c) and (d) are marked with cyan color.

From the outputs it can be noted that Adiposoft only shows decent output when adipocytes cover maximum area of a sample image (e.g. Figures 18 and 20). In a heterogeneous sample image this tool can tag many non-fat areas as valid fats (e.g. Figures 21, 22 and 24). Moreover, it can even fail to identify presence of any fat in an image (e.g. Figures 16 and 23). Hence, Fatquant performs better in the scenarios shown. The tagging of fat cells shown in (b) images are done by the authors and not collected from any laboratory. Ground truth data of the slides used was not officially made available by the source.

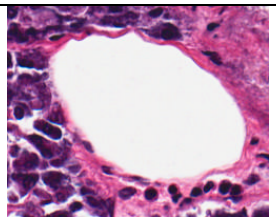

Figure 26 (a)-sample

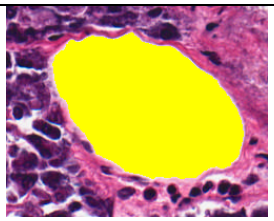

Figure 26 (b)-tagged

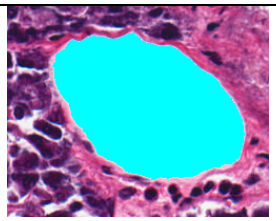

Figure 26 (c)-Fatquant

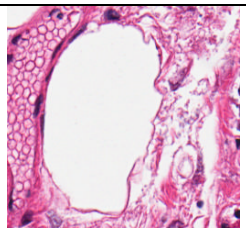

Figure 27 (a)-sample

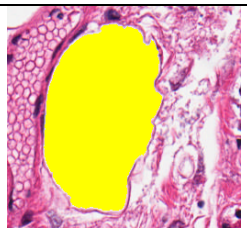

Figure 27 (b)-tagged

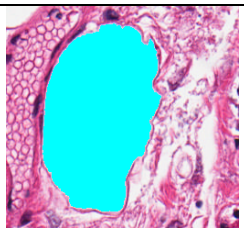

Figure 27 (c)-Fatquant

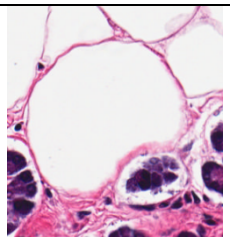

Figure 28 (a)-sample

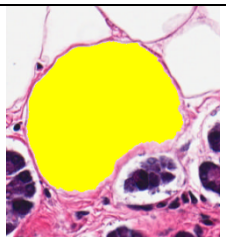

Figure 28 (b)-tagged

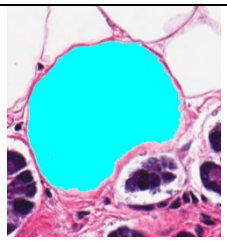

Figure 28 (c)-Fatquant

bioRxiv preprint doi: https://doi.org/10.1101/2021.12.13.472341; this version posted September 28, 2022. The copyright holder for this preprint (which was not certified by peer review) is the author/funder, who has granted bioRxiv a license to display the preprint in perpetuity. It is made available under aCC-BY 4.0 International license.

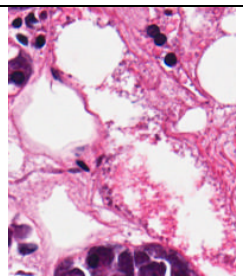

Figure 29 (a)-sample

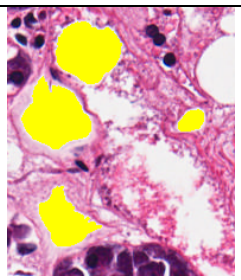

Figure 29 (b)-tagged

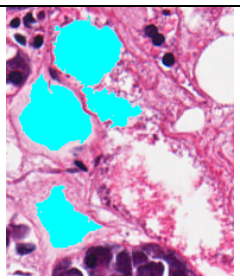

Figure 29 (c)-Fatquant

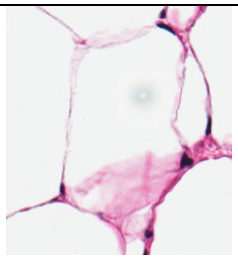

Figure 30 (a)-sample

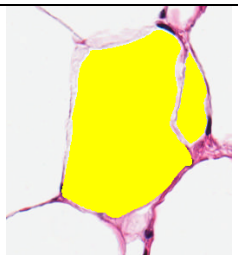

Figure 30 (b)-tagged

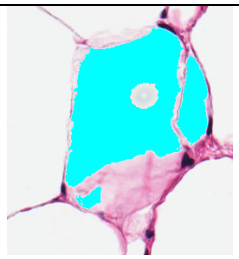

Figure 30 (c)-Fatquant

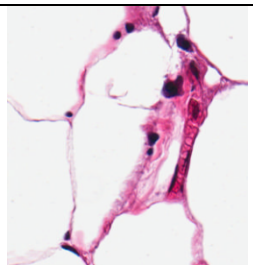

Figure 31 (a)-sample

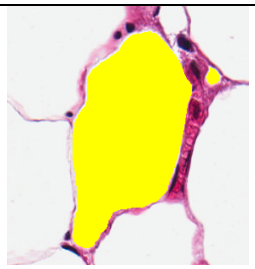

Figure 31 (b)-tagged

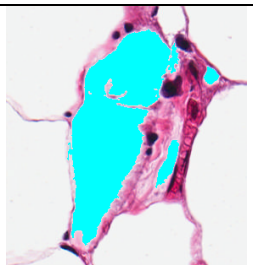

Figure 31 (c)-Fatquant

Table 5: Accuracy of machine annotation by Fatquant in Figures 26 – 31

Figures	GTEx slide ID	Threshold value	Min. diameter	Max. diameter	TP (in pixels)	FP (in pixels)	FN (in pixels)	IoU
26	117YW-0926	229	20	180	17640	118	102	0.987
27	1117F-1	227	30	200	19321	269	15	0.985

bioRxiv preprint doi: https://doi.org/10.1101/2021.12.13.472341; this version posted September 28, 2022. The copyright holder for this preprint (which was not certified by peer review) is the author/funder, who has granted bioRxiv a license to display the preprint in perpetuity. It is made available under aCC-BY 4.0 International license.

	726							
28	117YW-0926	228	20	200	26095	115	334	0.983
29	111VG-0926	227	35	100	5692	1312	326	0.776
30	117YW-0926	236	15	220	18178	499	7042	0.707
31	117YW-0926	231	10	200	16441	484	7623	0.670

Image (a) in Figures 26 – 31 are the sample images; (b) represents manual tagged and (c) represents machine tagged areas using Fatquant of images in (a). As per the data mentioned in Table 5 it can be noted that fat cells available in Figures 26 – 28 are easy to get tagged by this tool, hence IoU value increases. Whereas the tool does not detect fat cell properly when cell boundaries are not clearly delineated as seen in Figures 29 – 31, hence IoU value decreases. So validity analysis performed on sample images with many fat cells similar to that of Figures 26 – 28 will likely show higher accuracy. Manual tagged data shown in (b) images are not collected from any laboratory website and are rather created by the authors. So, there can be some variation in ground truth data of these images created by any other source. In the GitHub repository mentioned, sample images used in Figures 16 – 25 and Figures 26 – 31 are available in 'Test_samples' and 'Small_samples' directories respectively.

4. Discussion

Pancreatic fat accumulation has been associated with obesity, impaired b-cell function and may be an early sign in the development of metabolic syndrome (Dite et al 2020, Sequeira et al 2022,

bioRxiv preprint doi: https://doi.org/10.1101/2021.12.13.472341; this version posted September 28, 2022. The copyright holder for this preprint (which was not certified by peer review) is the author/funder, who has granted bioRxiv a license to display the preprint in perpetuity. It is made available under aCC-BY 4.0 International license.

Rugivarodom et al 2022). Pancreas is a heterogenous tissue and current tools for fat cell analysis such as Adiposoft (Galarraga et al 2012), AdipoCount (Zhi et al 2018) are unable to analyze fat cell infiltration in pancreas. Current automated pancreas tool are largely restricted to segmentation of the endocrine islet fractions of pancreas and are based on cell nulcei identification, extracting colour features mostly for pancreatic cancer detection (Huang et al 2016, Vu et al 2019, Yang et al 2021). There are other deep learning based methods for pancreas segmentation but again this are largely restricted to cancer diagnosis (Huang et al 2021) but cannot analyze fatty cell infiltration.

We have developed a tool, Fatquant, to identify fat cells in heterogeneous histological tissue sections that can complement work of pathologist in identification and analysis of fat cells due to their growing importance in pathophysiological functions and with the availability of whole slide digitized images it can save significant amount of time. Based on our analysis, Adiposoft shows decent output when adipocytes cover maximum area of a sample image and label non-fat areas as valid fat cells in heterogenous tissue sample images. In absence of ground truth images, we manually annotated fat cells in different pancreas sample images and then compared the output accuracy using IoU with Fatquant tool annotated results. We observed an IoU of 0.797 to 0.966 exhibiting high degree of similarity between manual versus Fatquant annotation. Our fatquant tool works well for both homogenous adipose tissue and varied heterogenous tissues like pancreas, liver suggesting diverse applicability of the tool for analysis of fat cells.

Acknowledgments

There is no potential conflicts of interest and no funding to declare. This research did not receive any specific grant from funding agencies in the public, commercial, or not-for-profit sectors.

bioRxiv preprint doi: https://doi.org/10.1101/2021.12.13.472341; this version posted September 28, 2022. The copyright holder for this preprint (which was not certified by peer review) is the author/funder, who has granted bioRxiv a license to display the preprint in perpetuity. It is made available under aCC-BY 4.0 International license.

References

1. Paul, J., & Shihaz, A. (2020). PANCREATIC STEATOSIS: A NEW DIAGNOSIS AND THERAPEUTIC CHALLENGE IN GASTROENTEROLOGY. *Arquivos de gastroenterologia*, *57*(2), 216–220. https://doi.org/10.1590/s0004-2803.202000000-27

2. Tariq, H., Nayudu, S., Akella, S., Glandt, M., & Chilimuri, S. (2016). Non-Alcoholic Fatty Pancreatic Disease: A Review of Literature. *Gastroenterology research*, *9*(6), 87–91. https://doi.org/10.14740/gr731w

3. Yu, T. Y., & Wang, C. Y. (2017). Impact of non-alcoholic fatty pancreas disease on glucose metabolism. *Journal of diabetes investigation*, *8*(6), 735–747. https://doi.org/10.1111/jdi.12665

4. Verma, A. R., & Papalois, V. (2011). Evaluating steatosis in pancreatic transplant. *Experimental and clinical transplantation : official journal of the Middle East Society for Organ Transplantation*, *9*(3), 159–164.

5. Dholakia, S., Sharples, E. J., Ploeg, R. J., & Friend, P. J. (2017). Significance of steatosis in pancreatic transplantation. *Transplantation reviews (Orlando, Fla.)*, *31*(4), 225–231. https://doi.org/10.1016/j.trre.2017.08.001

6. Lesmana, C.R.A., Pakasi, L.S., Inggriani, S. *et al.* Prevalence of Non-Alcoholic Fatty Pancreas Disease (NAFPD) and its risk factors among adult medical check-up patients in a private hospital: a large cross sectional study. *BMC Gastroenterol* **15,** 174 (2015). https://doi.org/10.1186/s12876-015-0404-1

7. Fukui, H., Hori, M., Fukuda, Y., Onishi, H., Nakamoto, A., Ota, T., Ogawa, K., Ninomiya, K., Tatsumi, M., Osuga, K., Yamada, D., Eguchi, H., Miyoshi, E., & Tomiyama, N. (2019). Evaluation of fatty pancreas by proton density fat fraction using 3-T magnetic resonance imaging and its association with pancreatic cancer. *European journal of radiology*, *118*, 25–31.

bioRxiv preprint doi: https://doi.org/10.1101/2021.12.13.472341; this version posted September 28, 2022. The copyright holder for this preprint (which was not certified by peer review) is the author/funder, who has granted bioRxiv a license to display the preprint in perpetuity. It is made available under aCC-BY 4.0 International license.

https://doi.org/10.1016/j.ejrad.2019.06.024

8. Virostko J. (2020). Quantitative Magnetic Resonance Imaging of the Pancreas of Individuals With Diabetes. *Frontiers in endocrinology*, *11*, 592349. https://doi.org/10.3389/fendo.2020.592349

9. Taylor, R., Al-Mrabeh, A., Zhyzhneuskaya, S., Peters, C., Barnes, A. C., Aribisala, B. S., Hollingsworth, K. G., Mathers, J. C., Sattar, N., & Lean, M. (2018). Remission of Human Type 2 Diabetes Requires Decrease in Liver and Pancreas Fat Content but Is Dependent upon Capacity for β Cell Recovery. *Cell metabolism*, *28*(4), 547–556.e3. https://doi.org/10.1016/j.cmet.2018.07.003

10. Gurcan, M. N., Boucheron, L. E., Can, A., Madabhushi, A., Rajpoot, N. M., & Yener, B. (2009). Histopathological image analysis: a review. *IEEE Rev Biomed Eng, 2*, 147-171. doi: 10.1109/RBME.2009.2034865.

11. Galarraga, M., Campion, J., Munoz-Barrutia, A., Boque, N., Moreno, H., Martinez, J. A., . . . Ortiz-de-Solorzano, C. (2012). Adiposoft: automated software for the analysis of white adipose tissue cellularity in histological sections. *J Lipid Res, 53*(12), 2791-2796. doi: 10.1194/jlr.D023788.

12. Zhi, X., Wang, J., Lu, P., Jia, J., Shen, H. B., & Ning, G. (2018). AdipoCount: A New Software for Automatic Adipocyte Counting. *Front Physiol, 9*, 85. doi: 10.3389/fphys.2018.00085.

bioRxiv preprint doi: https://doi.org/10.1101/2021.12.13.472341; this version posted September 28, 2022. The copyright holder for this preprint (which was not certified by peer review) is the author/funder, who has granted bioRxiv a license to display the preprint in perpetuity. It is made available under aCC-BY 4.0 International license.

13. Glastonbury, C. A., Pulit, S. L., Honecker, J., Censin, J. C., Laber, S., Yaghootkar, H., . . . Lindgren, C. M. (2020). Machine Learning based histology phenotyping to investigate the epidemiologic and genetic basis of adipocyte morphology and cardiometabolic traits. *PLoS Comput Biol, 16*(8), e1008044. doi: 10.1371/journal.pcbi.1008044.

14. Nativ, N. I., Chen, A. I., Yarmush, G., Henry, S. D., Lefkowitch, J. H., Klein, K. M., Maguire, T. J., Schloss, R., Guarrera, J. V., Berthiaume, F., & Yarmush, M. L. (2014). Automated image analysis method for detecting and quantifying macrovesicular steatosis in hematoxylin and eosin-stained histology images of human livers. *Liver transplantation : official publication of the American Association for the Study of Liver Diseases and the International Liver Transplantation Society*, *20*(2), 228–236. https://doi.org/10.1002/lt.23782

15. Catanzaro, R., Cuffari, B., Italia, A., & Marotta, F. (2016). Exploring the metabolic syndrome: Nonalcoholic fatty pancreas disease. *World journal of gastroenterology*, *22*(34), 7660–7675. https://doi.org/10.3748/wjg.v22.i34.7660

16. Matsuda, A., Makino, N., Tozawa, T., Shirahata, N., Honda, T., Ikeda, Y., Sato, H., Ito, M., Kakizaki, Y., Akamatsu, M., Ueno, Y., & Kawata, S. (2014). Pancreatic fat accumulation, fibrosis, and acinar cell injury in the Zucker diabetic fatty rat fed a chronic high-fat diet. *Pancreas*, *43*(5), 735–743. https://doi.org/10.1097/MPA.0000000000000129

17. Apaolaza, P. S., Petropoulou, P. I., & Rodriguez-Calvo, T. (2021). Whole-Slide Image Analysis of Human Pancreas Samples to Elucidate the Immunopathogenesis of Type 1 Diabetes Using the QuPath Software. *Frontiers in molecular biosciences*, *8*, 689799. https://doi.org/10.3389/fmolb.2021.689799

bioRxiv preprint doi: https://doi.org/10.1101/2021.12.13.472341; this version posted September 28, 2022. The copyright holder for this preprint (which was not certified by peer review) is the author/funder, who has granted bioRxiv a license to display the preprint in perpetuity. It is made available under aCC-BY 4.0 International license.

18. Floros, X., Fuchs, T. J., Rechsteiner, M. P., Spinas, G., Moch, H., & Buhmann, J. M. (2009). Graph-based pancreatic islet segmentation for early type 2 diabetes mellitus on histopathological tissue. *Medical image computing and computer-assisted intervention : MICCAI ... International Conference on Medical Image Computing and Computer-Assisted Intervention*, *12*(Pt 2), 633–640. https://doi.org/10.1007/978-3-642-04271-3_77

19. Rechsteiner, M. P., Floros, X., Boehm, B. O., Marselli, L., Marchetti, P., Stoffel, M., Moch, H., & Spinas, G. A. (2014). Automated assessment of β-cell area and density per islet and patient using TMEM27 and BACE2 immunofluorescence staining in human pancreatic β-cells. *PloS one*, *9*(6), e98932. https://doi.org/10.1371/journal.pone.0098932

20. Huang, Y., Liu, C., Eisses, J. F., Husain, S. Z., & Rohde, G. K. (2016). A supervised learning framework for pancreatic islet segmentation with multi-scale color-texture features and rolling guidance filters. *Cytometry. Part A : the journal of the International Society for Analytical Cytology*, *89*(10), 893–902. https://doi.org/10.1002/cyto.a.22929

21. Consortium, G. TEx. (2015). Human genomics. The Genotype-Tissue Expression (GTEx) pilot analysis: multitissue gene regulation in humans. *Science, 348*(6235), 648-660. doi: 10.1126/science.1262110.

22. Badea, L., & Stanescu, E. (2020). Identifying transcriptomic correlates of histology using deep learning. *PLoS One, 15*(11), e0242858. doi: 10.1371/journal.pone.0242858.

23. Roy, M., Wang, F., Vo, H., Teng, D., Teodoro, G., Farris, A. B., Castillo-Leon, E., Vos, M. B.,

bioRxiv preprint doi: https://doi.org/10.1101/2021.12.13.472341; this version posted September 28, 2022. The copyright holder for this preprint (which was not certified by peer review) is the author/funder, who has granted bioRxiv a license to display the preprint in perpetuity. It is made available under aCC-BY 4.0 International license.

& Kong, J. (2020). Deep-learning-based accurate hepatic steatosis quantification for histological assessment of liver biopsies. *Laboratory investigation; a journal of technical methods and pathology*, *100*(10), 1367–1383. https://doi.org/10.1038/s41374-020-0463-y

24. Dite, P., Blaho, M., Bojkova, M., Jabandziev, P., & Kunovsky, L. (2020). Nonalcoholic Fatty Pancreas Disease: Clinical Consequences. *Digestive diseases (Basel, Switzerland)*, *38*(2), 143–149. https://doi.org/10.1159/000505366

25. Sequeira, I. R., Yip, W. C., Lu, L., Jiang, Y., Murphy, R., Plank, L. D., Cooper, G., Peters, C. N., Lu, J., Hollingsworth, K. G., & Poppitt, S. D. (2022). Pancreas Fat, an Early Marker of Metabolic Risk? A Magnetic Resonance Study of Chinese and Caucasian Women: TOFI_Asia Study. *Frontiers in physiology*, *13*, 819606. https://doi.org/10.3389/fphys.2022.819606

26. Rugivarodom, M., Geeratragool, T., Pausawasdi, N., Charatcharoenwitthaya, P. (2022). Fatty Pancreas: Linking Pancreas Pathophysiology to Nonalcoholic Fatty Liver Disease. *J Clin Transl Hepatol*. 1-11. doi: 10.14218/JCTH.2022.00085.

27. Vu, Q. D., Graham, S., Kurc, T., To, M., Shaban, M., Qaiser, T., Koohbanani, N. A., Khurram, S. A., Kalpathy-Cramer, J., Zhao, T., Gupta, R., Kwak, J. T., Rajpoot, N., Saltz, J., & Farahani, K. (2019). Methods for Segmentation and Classification of Digital Microscopy Tissue Images. *Frontiers in bioengineering and biotechnology*, *7*, 53. https://doi.org/10.3389/fbioe.2019.00053

27. Yang, C., Xiang, D., Bian, Y., Lu, J., Jiang, H., Zheng, J. (2021). Gland segmentation in pancreas histopathology images based on selective multi-scale attention. Proc. SPIE 11596,

bioRxiv preprint doi: https://doi.org/10.1101/2021.12.13.472341; this version posted September 28, 2022. The copyright holder for this preprint (which was not certified by peer review) is the author/funder, who has granted bioRxiv a license to display the preprint in perpetuity. It is made available under aCC-BY 4.0 International license.

Medical Imaging 2021: Image Processing, 115962M (15 February 2021); https://doi.org/10.1117/12.2581039

28. Huang, M., Huang, C., Yuan, J., & Kong, D. (2021). A Semiautomated Deep Learning Approach for Pancreas Segmentation. *Journal of healthcare engineering*, *2021*, 3284493. https://doi.org/10.1155/2021/3284493